



Article

Effects of Number of Atoms and Doping Concentration on the Structure, Phase Transition, and Crystallization Process of $\text{Fe}_{1-x-y}\text{Ni}_x\text{Co}_y$ Alloy: A Molecular Dynamic Study

Dung Nguyen Trong ¹, Van Cao Long ¹ and Ștefan Țălu ^{2,*}¹ Institute of Physics, University of Zielona Góra, Prof. Szafrana 4a, 65-516 Zielona Góra, Poland² The Directorate of Research, Development and Innovation Management (DMCDI), Technical University of Cluj-Napoca, 15 Constantin Daicoviciu St., 400020 Cluj-Napoca, Cluj County, Romania

* Correspondence: stefan_ta@yahoo.com or stefan.talu@auto.utcluj.ro

Abstract: In this study, molecular dynamics simulations are employed to study the influencing factors such as doping concentration, number of atoms, and temperature on the structural characteristics, phase transition, and crystallization of $\text{Fe}_{1-x-y}\text{Ni}_x\text{Co}_y$ alloy. The results show that $\text{Fe}_{1-x-y}\text{Ni}_x\text{Co}_y$ alloy always exists with three metals, Fe, Ni, and Cu, which are distributed quite evenly according to the ratio of tap phase concentration. In $\text{Fe}_{1-x-y}\text{Ni}_x\text{Co}_y$ alloy, there are always six types of links, Fe–Fe, Fe–Ni, Fe–Co, Ni–Ni, Ni–Co, and Co–Co. Calculated results showed with the increases in the doping concentration, the length of links (r) has a constant value and the height $g(r)$ of the Radial Distribution Function (RDF) has a modified value. The process of increasing the concentration of Fe doping, and reducing the concentration of Co doping leads to an increase in crystallization, a decrease in the size (l) of the alloy, and the total energy of the system (E_{tot}) increases and then decreases. Similarly, increasing the number of atoms leads to an increase in crystallization, but with an increase in temperature, the crystallization process decreases (that corresponds to the change in the number of structural units for the Face-centered cubic (FCC), Hexagonal Close-Packed (HCP), Body-centered cubic (BCC), and Amorphous (Amor)). The obtained results serve as a basis for experimental research in developing new magnetic materials in the future.

Keywords: crystallization process; doping concentration; $\text{Fe}_{1-x-y}\text{Ni}_x\text{Co}_y$ alloy; molecular dynamics; number of atoms; phase transition; structure; temperature



Citation: Trong, D.N.; Long, V.C.; Țălu, Ș. Effects of Number of Atoms and Doping Concentration on the Structure, Phase Transition, and Crystallization Process of $\text{Fe}_{1-x-y}\text{Ni}_x\text{Co}_y$ Alloy: A Molecular Dynamic Study. *Appl. Sci.* **2022**, *12*, 8473. <https://doi.org/10.3390/app12178473>

Academic Editor: Leonid Burakovsky

Received: 30 July 2022

Accepted: 23 August 2022

Published: 25 August 2022

Publisher's Note: MDPI stays neutral with regard to jurisdictional claims in published maps and institutional affiliations.



Copyright: © 2022 by the authors. Licensee MDPI, Basel, Switzerland. This article is an open access article distributed under the terms and conditions of the Creative Commons Attribution (CC BY) license (<https://creativecommons.org/licenses/by/4.0/>).

1. Introduction

In recent decades, a major direction from materials science focuses on understanding and applying the properties of matter to develop new multi-component alloys, with improved physical and chemical properties, based on advanced technological methods. In the literature, there are various studies on multi-component alloys (such as grain growth [1], single-phase high-entropy alloys [2], non-equiatomic high-entropy alloys [3], phase stability of equiatomic high-entropy alloys [4], tensile properties of dual-phase high-entropy alloys [5], and so on). On the other hand, it is known that multi-component alloys are considered good candidates to improve the entropy coefficient. In 2004, for the first time, nanostructured high-entropy alloys with multiple principal elements were proposed by Yeh et al. [6] and Cantor et al. [7], and for the first time, scientists made extensive investigations on the maximum value of a high entropy alloy [8]. A number of studies have suggested that high-entropy alloys have unique properties in a variety of applications [9–11]. These new findings prompted researchers to explore medium-entropy alloys (MEAs) such as CoCrNi (three-component alloys), that exhibit superior strength to CoCrFeMnNi alloy [12–15]. In the literature, there are different studies aimed at the mechanical properties of low entropy alloys [6,8,10,12,14,16]. However, so far, only a few studies have used transition metals, such as Fe [17,18], Ni [19,20], Al [21], and Cu [22], in magnetism,

thermal, shape memory, soft elastomers, and electrical materials (such as CoCrFeMnNi that exhibits highly complex low-temperature magnetic properties [23]). Recently, scientists have identified the effects of high entropy of mixing and low mixing temperatures, associated with alloys that can form solid solutions randomly in a structural phase, such as Face-centered cubic (FCC) or Body-centered cubic (BCC). In other studies, extensive experimental investigations on high entropy alloys were conducted [24], (e.g., an integrated electromagnetic inductor with FeNiCo [25], FeNiCoCrMn, and its subset [26,27]). Besides the results of the experimental method, there is also a simulation method that plays a great role in the success of studying the properties of new materials. Among the simulation methods, there is Density Functional Theory (DFT) methods, Monte-Carlo (MC) methods, and Molecular Dynamics (MD) simulation methods. With the specified methods, the MD method plays a key role, because of its simplicity. This method, which has been used by researchers since the 1950s [28], was only developed in 1980 thanks to the first IPM computer system. To this day, this method is strongly developed thanks to supercomputer systems combined with theoretical models of solids [29] and has been proven in various studies [30]. In studies based on the simulation method, researchers are always interested in issues such as the stability of materials, and whether the selection of parameters that will be put into the model is consistent with the experimental results. In addition, scientists are also interested in issues such as the sensitive dependence of the initial conditions leading to chaos, and the accuracy of the integration method for the system of large nonlinear partial differential equations [31]. Scientists have published various studies concerning structural characteristics, phase transition, crystallization process, and mechanical and magnetic properties of 2-component alloys (such as NiFe nanoparticles [32], NiCu [33–35], AlNi nanoparticles [36], AgAu alloy [37], AuCu bulk [38,39], NiAu alloy [40] and polymer [41], and Fe₂O₃ [42,43]). In the obtained results, the authors have successfully determined the lengths of links of the Fe–Fe, and Fe–Ni. For example, with the simulation method $r_{\text{Fe-Fe}} = 2.55 \text{ \AA}$ [17,18,44–46] for amorphous Fe; $r_{\text{Ni-Ni}} = 2.45 \text{ \AA}$ [19,20] for Ni crystallization; $r_{\text{Fe-Ni}} = 2.47 \text{ \AA}$ [32]; and 2.48 \AA [47] with 2-component alloys. The following results were obtained based on the experimental method ($r_{\text{Fe-Fe}} = 2.54 \text{ \AA}$ [48]); with the neutron method ($r_{\text{Fe-Fe}} = 2.62 \text{ \AA}$ [49]); with the X-ray method for amorphous Fe ($r_{\text{Fe-Fe}} = 2.57 \text{ \AA}$ [50]); and with the two-component alloys ($r_{\text{Fe-Ni}} = 2.53 \text{ \AA}$ [51]). Currently, scientists have increased the number of components in the alloy to 3 metals and they used experimental methods to study the structural and magnetic properties of the FeCoNi alloy [52]. However, structural features such as bond lengths, number of structural units, shape and phase transitions, and crystallization have not yet been determined. In this research, we apply the method of molecular dynamics to study the structural characteristics, phase transition, and crystallization of the Fe_{1-x-y}Ni_xCo_y alloy, in order to elucidate the cause of the alloy's magnetic properties and to facilitate the experimental process.

2. Method of Calculation

Initially, we sow randomly atoms of Fe_{1-x-y}Ni_xCo_y alloy with a ratio into a cube of size (l) determined, and it was applied the following formula (1):

$$l = \sqrt[3]{\frac{N}{\rho}} = \sqrt[3]{\frac{(m_{\text{Fe}} \cdot n_{\text{Fe}} + m_{\text{Ni}} \cdot n_{\text{Ni}} + m_{\text{Co}} \cdot n_{\text{Co}})}{\rho}} \quad (1)$$

where: l, N, ρ is the size, the number of atoms, and the density of atoms, respectively, and m_{Fe} , n_{Fe} , and m_{Ni} , n_{Ni} , m_{Co} , n_{Co} is molar mass atomic and number of atoms of Fe, Ni, Co metals, respectively.

To study the structural features, phase transitions, and crystallization, we use LAMMPS open-source software [37,53,54] based on the molecular dynamics simulation (MD) method, suitable for periodic boundary conditions and Sutton–Chen embedded force field (2) [53–56]:

$$F_i(\rho) = A_i E_i^0 \rho \ln \rho; \rho_i^{a(1)}(R) = e^{-b^*}, \quad b^* = \beta_i^{(1)} \left(\frac{R}{R_i^0 - 1} \right), \quad \left(\frac{\rho}{\rho_i} \right)^2 = \sum_{l=0}^3 t_l^{(1)} \left(\rho_i^{(1)} \right)^2 \quad (2)$$

This is a high-precision embedded interaction potential field for the study of structural characteristics for Fe, Ni, and Co single-component metals [19,20,57], and 2-component alloys [32,47]. Considering interaction force fields [58–63] from the physical system can be investigated comprehensively the energy, phase stability, hole formation, and surface binding energy. It is known that for the metal 1 ingredient (that always has the FCC structure stable, and electron density is associated at equilibrium with the value of 1), the derivative of the interaction function will be always 0 to maximize entropy.

To perform the simulation, we use the parameters of $\text{Fe}_{1-x-y}\text{Ni}_x\text{Co}_y$ alloy (corresponding to the values of the component metals Fe, Ni, and Co in Tables 1–3 of references [56,64]). First, we combined the process of running 2×10^4 step recovery statistics of MD simulation at temperature (T), $T = 4500$ K so that the atoms are in the initial steady state. Then, it is decreased the temperature from $T = 4500$ K to $T = 1300$ K, 1100 K, 900 K, 800 K, 700 K, 600 K, 500 K, 400 K, and 300 K (to increase the crystallization state with 42×10^4 MD steps, heating rate 4×10^{11} K/s, and a heating step of 1 fs). In this way, are studied the influence of Fe, Ni, and Co doping concentrations corresponding to alloys $\text{Fe}_5\text{Ni}_{32}\text{Co}_{63}$, $\text{Fe}_{33.4}\text{Ni}_{33.3}\text{Co}_{33.3}$, $\text{Fe}_{63}\text{Ni}_{32}\text{Co}_5$; associated with number of atoms (N), ($N = 2916$ atoms, 5324 atoms, 8788 atoms, 13,500 atoms of $\text{Fe}_{63}\text{Ni}_{32}\text{Co}_5$ alloy), and temperature (T), respectively.

To study the structure characteristics quantities through structure shape, and size (l), the Radial Distribution Function (RDF) formula is applied (3) [65]:

$$g(r) = \frac{V}{N^2} \left\langle \frac{\sum_i n_i(r)}{4\pi r^2 \Delta r} \right\rangle \quad (3)$$

where: r , $n_i(r)$, V , N , and $g(r)$ are the link length, the coordinates, the volume, the number of atoms, and the radial distribution function, respectively. Moreover, $g(r)$ is noted as the density value of the maximum probability of finding the atoms at the first peak of the RDF [66].

To determine the diffusion mechanism of the atoms, we used the Mean Squared Distance (MSD) method (3) [67]. Furthermore, to visualize the structure, phase transition, and crystallization of the alloy, we used the open source software OVITO [63,68] (to determine the RDF, structure shape, and the number of structural unit positions based on Common Neighbor Analysis (CNA) [69–74]). It is known that all alloys are made through phase transitions and the Nosé [75] and Hoover [76] laws can be applied in experimental and computational studies. Finally, to check the accuracy of the results, the Displacement Analysis (DXA) was used [68].

3. Results and Discussion

3.1. Characteristic Quantities

Initially, the $\text{Fe}_{1-x-y}\text{Ni}_x\text{Co}_y$ alloy, $x = 0.32$, $y = 0.05$ ($\text{Fe}_{63}\text{Ni}_{32}\text{Co}_5$) with 13,500 atoms corresponding to 8505 Fe atoms, 4320 Ni atoms, and 675 Co atoms were set at $T = 4500$ K, $P = 0$ GPa, for recovery statistics, with 2×10^4 steps, simulation step time is 1 fs, and heating rate 4×10^{11} K/s (to obtain initial stabilization for the studied material). Characteristic quantities, structure, phase transition, and crystallization are shown in Figure 1.

The obtained results show that at temperature (T), $T = 300$ K, the $\text{Fe}_{63}\text{Ni}_{32}\text{Co}_5$ alloy has the shape of a cube, composed of 03 metals Fe (green), Ni (violet), Co (black), fairly evenly distributed, arranged in an orderly manner (Figure 1a). In addition, there are structural characteristic quantities such as the structured shape (Figure 1b) composed of 04 structural units: Face-centered cubic (FCC) has a red color, Hexagonal Close-Packed (HCP) is blue, Body-centered cubic (BCC) is black, and Amorphous (Amor) is yellow. The radial distribution function has links Fe–Fe, Fe–Ni, Fe–Co, Ni–Ni, Ni–Co, Co–Co corresponding to the lengths of the links $r_{\text{Fe-Fe}} = r_{\text{Fe-Ni}} = r_{\text{Fe-Co}} = r_{\text{Ni-Ni}} = r_{\text{Ni-Co}} = r_{\text{Co-Co}} = 2.475$ Å. The obtained results are completely consistent with previous simulation results (such as with bond lengths Fe–Fe, Ni–Ni, Fe–Ni, where the corresponding value is $r_{\text{Fe-Fe}} = 2.55$ Å [17,18,44–46] for amorphous Fe; $r_{\text{Ni-Ni}} = 2.45$ Å [19,20] for Ni crystallization; and $r_{\text{Fe-Ni}} = 2.47$ Å [32], 2.48 Å [47] with 2-component alloys). Based on the experimental method $r_{\text{Fe-Fe}} = 2.54$ Å [48];

$r_{\text{Fe-Fe}} = 2.62 \text{ \AA}$ [49] with the neutron method; $r_{\text{Fe-Fe}} = 2.57 \text{ \AA}$ [50] with X-ray method for amorphous Fe; with two component alloys $r_{\text{Fe-Ni}} = 2.53 \text{ \AA}$ [51]. Our computational results are completely consistent with the bond lengths of crystalline metals and have a smaller value for metals in the amorphous state. Currently, there are no studies about the structural characteristics of 3-component alloys. The authors will compare the lengths of the bonds with the bond lengths of the previous 1-component metal or 2-component alloy. Due to the electronic interaction, the lattice constant values of these three-component alloys are approximately equal and in addition, all are ferromagnetic. Moreover, the height $g(r)$ of the radial distribution function (RDF) is $g(r)_{\text{Fe-Fe}} = 8.12$, $g(r)_{\text{Fe-Ni}} = 7.32$, $g(r)_{\text{Fe-Co}} = 8.20$, $g(r)_{\text{Ni-Ni}} = 6.92$, $g(r)_{\text{Ni-Co}} = 7.34$, $g(r)_{\text{Co-Co}} = 6.76$ (Figure 1c). In which, the height $g(r)$ of the radial distribution function (correlation function) is the probability density function of finding the atom in the coordination number circle [66]. Correspondingly, the number of structural units associated with $\text{Fe}_{63}\text{Ni}_{32}\text{Co}_5$ alloy is 7290 FCC, 4860 HCP, 364 BCC, and 986 Amor (Figure 1d). In addition, at $T = 300 \text{ K}$, $P = 0 \text{ GPa}$, the size of the alloy (l) corresponds to $l = 5.33 \text{ nm}$, the total energy of the system (E_{tot}), $E_{\text{tot}} = -58,263 \text{ eV}$. The specific results for the structure of the $\text{Fe}_{63}\text{Ni}_{32}\text{Co}_5$ alloy, allow us to study the influencing factors in the following sections.

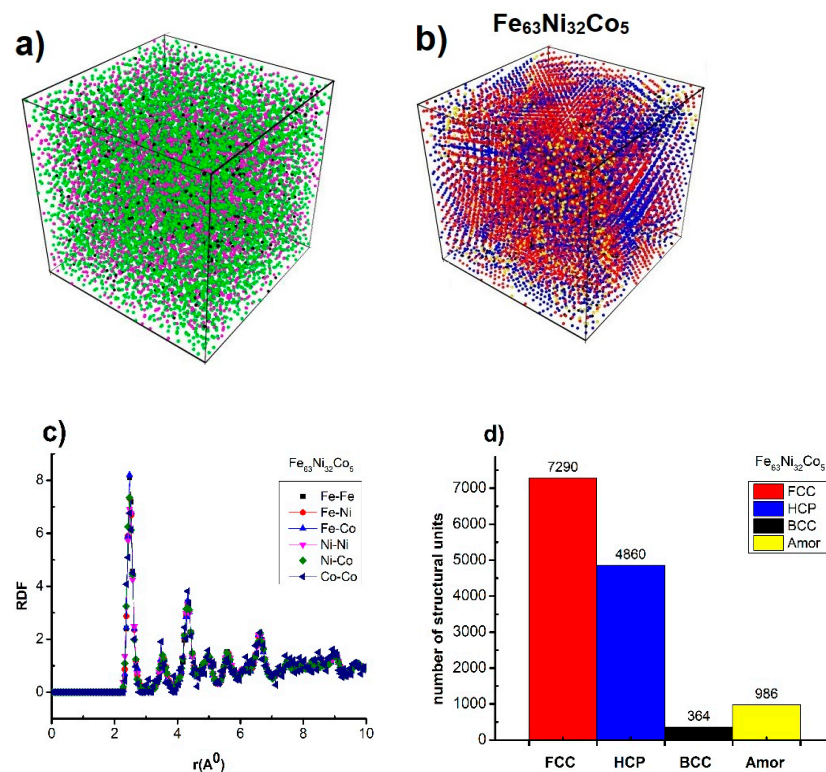


Figure 1. Shape (a), structure shape (b), RDF (c), number of structural unit (d) of $\text{Fe}_{63}\text{Ni}_{32}\text{Co}_5$ alloy at $T = 300 \text{ K}$.

3.2. Factors Affecting

In order to determine the factors affecting the structure, phase transition, and crystallization process of materials, the authors focus on studying quantities such as structure shape, radial distribution function, and the number of the structural unit.

3.2.1. Effect of Doping Concentration

The obtained results show that, at temperature (T), $T = 300 \text{ K}$, $P = 0 \text{ GPa}$, the $\text{Fe}_{1-x-y}\text{Ni}_x\text{Co}_y$ alloy with 13,500 atoms associated with $x = 0.32$, $y = 0.63$ ($\text{Fe}_5\text{Ni}_{32}\text{Co}_{63}$) has 13,500 atoms (corresponding to 8505 Fe atoms, 4320 Ni atoms and 675 Co atoms), and its structure shape is shown in Figure 2a1. For this case, the lengths of the links $r = 2.475 \text{ \AA}$ and the $g(r)$ of RDF is $g(r)_{\text{Fe-Ni}} = 7.01$, $g(r)_{\text{Fe-Co}} = 7.19$, and $g(r)_{\text{Ni-Co}} = 7.35$ (Figure 2b1). The number of the

structural unit is 7060 FCC, 4460 HCP, 575 BCC, and 1405 Amor as it is shown in Figure 2c1, the size of the alloy (l) corresponds to $l = 5.34$ nm, and the total energy of the system (E_{tot}), $E_{\text{tot}} = -58,189$ eV. When changes $x = y$ (corresponding to $x = y = 0.333$) ($\text{Fe}_{33.4}\text{Ni}_{33.3}\text{Co}_{33.3}$), and $x = 0.32$, $y = 0.05$ ($\text{Fe}_{63}\text{Ni}_{32}\text{Co}_5$), the concentration of doped Fe increases, Co decreases corresponding to the number of atoms. The Fe, Ni, Co, and structural shape change major (Figure 2a1–a3). Similarly, links lengths do not change $r = 2.475$ Å and the $g(r)$ of RDF varies greatly between $g(r)_{\text{Fe-Ni}} = 6.42$ to $g(r)_{\text{Fe-Ni}} = 7.32$, $g(r)_{\text{Fe-Co}} = 6.60$ to $g(r)_{\text{Fe-Co}} = 8.20$, $g(r)_{\text{Ni-Co}} = 6.97$ to $g(r)_{\text{Ni-Co}} = 7.35$ (Figure 2b1–b3). Furthermore, with the increase of impurities Fe or Co both lead to an increase in $g(r)$, which proves that Fe, Co metal has a smaller lattice constant than Ni metal (making honey larger atoms). In addition, the number of the structural unit varies greatly, corresponding to FCC decreasing and increasing, HCP increasing and decreasing, BCC increasing and decreasing, and Amor increasing and decreasing (Figure 2c1–c3) resulting in a change in the size of the alloy (l) that decreases from $l = 5.34$ to $l = 5.33$ nm, and the total energy of the system (E_{tot}) increases and then decreases from $E_{\text{tot}} = -58,189$ eV to $-57,932$ and $-58,263$ eV. The obtained results show that, when it is changed the doping concentration, the number of FCC, BCC, and Amor structural units increases (in $\text{Fe}_5\text{Ni}_{32}\text{Co}_{63}$, and $\text{Fe}_{63}\text{Ni}_{32}\text{Co}_5$), which shows the fact when increasing the concentration of Fe, Co doping leads to $\text{Fe}_{1-x-y}\text{Ni}_x\text{Co}_y$ alloy crystallization increases, but when increases the concentration of Ni doping, crystallization decreases. This is a difficult question for researchers as to why the difference in the crystallization process occurs when these metals are all magnetic metals, with nearly equal lattice constants. After the research process, we found that the root cause of this problem is caused by the electronic interaction between metals. In addition, with $\text{Fe}_{63}\text{Ni}_{32}\text{Co}_5$, there is the largest crystallization (corresponding to the total binding energy of the system that has the smallest value). The obtained results have an important impact on future experimental studies on the influence of doping concentration with 3-metal alloys. We choose $\text{Fe}_{63}\text{Ni}_{32}\text{Co}_5$ alloy as the standard material to investigate the influencing factors in the next section.

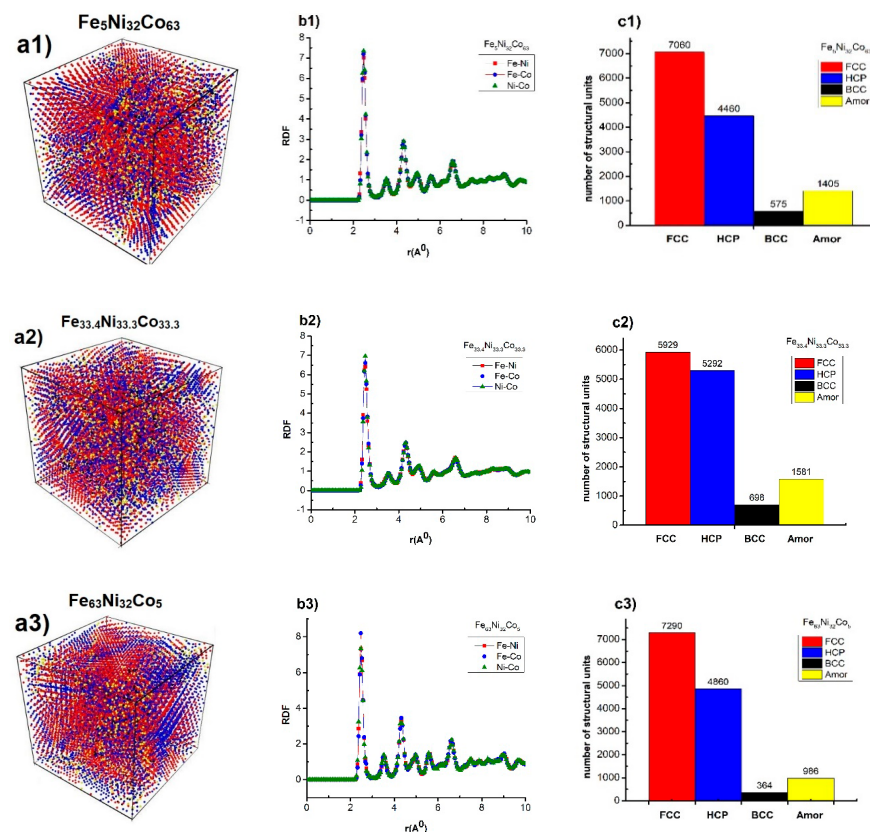


Figure 2. Structure shape (a1–a3), RDF (b1–b3), number of the structural unit (c1–c3) of $\text{Fe}_{1-x-y}\text{Ni}_x\text{Co}_y$ alloy at $T = 300$ K, $P = 0$ GPa with different adulteration.

3.2.2. Effect of Number of Atoms

The obtained results show that, at temperature (T), $T = 300$ K, $P = 0$ GPa the $\text{Fe}_{63}\text{Ni}_{32}\text{Co}_5$ alloy with 2916 atoms has the structure shape (Figure 3a1), the lengths of the links $r_{\text{Fe-Ni}} = r_{\text{Ni-Co}} = 2.475$ Å, $r_{\text{Fe-Co}} = 2.525$ Å and the $g(r)$ of RDF is $g(r)_{\text{Fe-Ni}} = 8.28$, $g(r)_{\text{Fe-Co}} = 7.20$, $g(r)_{\text{Ni-Co}} = 8.25$ (Figure 3b1). The number of the structural unit of FCC, HCP, BCC, Amor (Figure 3c1), and the size of the alloy (l) corresponds to $l = 3.20$ nm, the total energy of the system (E_{tot}), $E_{\text{tot}} = -12,657$ eV. When it is increased the number of atoms from $N = 2916$ atoms to $N = 5324$, 8788, 13,500 atoms, the shape of the structure changes greatly, corresponding to an increase in the density of structural atoms (Figure 3a1–a4). At the same time, $r_{\text{Fe-Ni}} = r_{\text{Ni-Co}} = 2.475$ Å, especially for $r_{\text{Fe-Co}}$ when decreases from $r_{\text{Fe-Co}} = 2.525$ Å to $r_{\text{Fe-Co}} = 2.475$ Å; also, $g(r)$ of RDF changed, the $g(r)_{\text{Fe-Ni}}$ changed down in the range from $g(r)_{\text{Fe-Ni}} = 8.28$ to $g(r)_{\text{Fe-Ni}} = 7.01$; $g(r)_{\text{Fe-Co}}$ changes up from $g(r)_{\text{Fe-Co}} = 6.40$ to $g(r)_{\text{Fe-Co}} = 8.20$; $g(r)_{\text{Ni-Co}}$ varies from $g(r)_{\text{Ni-Co}} = 8.25$ to $g(r)_{\text{Ni-Co}} = 5.97$ (Figure 3b1–b4) and number of structural unit of FCC increased from 1741 FCC to 7290 FCC, HCP increased from 1063 HCP to 4860 HCP, BCC increased from 18 BCC to 364 BCC, Amor increased from 94 Amor to 986 Amor (Figure 3c1–c4), and the size of the alloy (l) corresponds to an increase from $l = 3.20$ nm to $l = 5.34$ nm; the total energy of the system (E_{tot}) decreases from $E_{\text{tot}} = -12,657$ eV to $E_{\text{tot}} = -58,263$ eV. The obtained results show that when increased the number of atoms leads to structural units FCC, HCP, BCC increase, and Amor decreases (the cause of increased crystallization is by the size effect cause). We choose $\text{Fe}_{63}\text{Ni}_{32}\text{Co}_5$ alloy with 13,500 atoms as the standard material to investigate influencing factors in the next section.

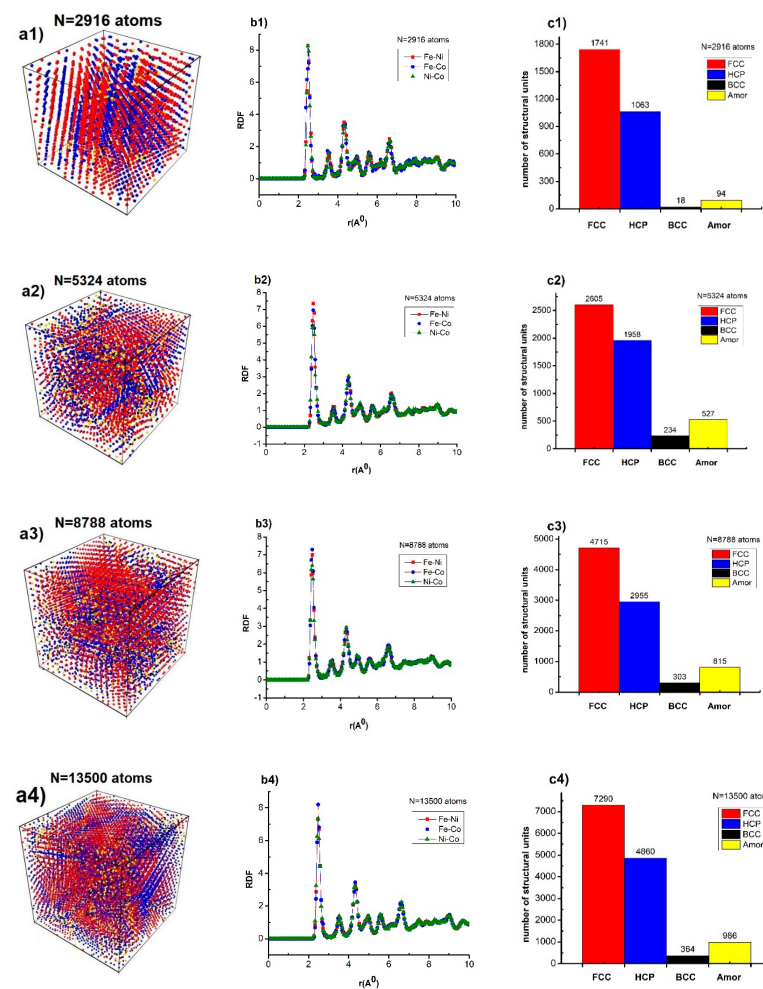


Figure 3. Structure shape (a1–a4), RDF (b1–b4), number of structural unit (c1–c4) of $\text{Fe}_{63}\text{Ni}_{32}\text{Co}_5$ alloy at $T = 300$ K, $P = 0$ GPa with different numbers of atoms.

3.2.3. Effect of Temperature

Similarly, to determine the effect of temperature on the structure, through the phase transition and crystallization process of $\text{Fe}_{63}\text{Ni}_{32}\text{Co}_5$ alloy, we only need to investigate the total energy value of the system and the number of crystal structure units of materials at the respective temperature. The obtained results are shown in Table 1.

Table 1. Parameters associated with the structure of $\text{Fe}_{63}\text{Ni}_{32}\text{Co}_5$ alloy with 13,500 atoms at different temperatures.

Temperature (K)	300	500	700	900	1100	1300
E_{tot} (eV)	−58,263	−57,941	−57,610	−57,275	−56,938	−56,630
Number of crystalline structure units	12,514	12,496	12,462	12,389	12,306	12,137

The obtained results show that, at temperature (T), $T = 300$ K, $P = 0$ GPa, the $\text{Fe}_{63}\text{Ni}_{32}\text{Co}_5$ alloy with 13,500 atoms have the lengths of the links with a constant value $r = 2.475$ Å, and the $g(r)$ of RDF changes in a corresponding way. In addition, the number of crystalline structure units (FCC, HCP, BCC) is 12,514 atoms; the size of the alloy (l) corresponds to $l = 5.34$ nm, the total energy of the system (E_{tot}), $E_{\text{tot}} = -58,263$ eV. When increasing the temperature from $T = 300$ K to $T = 500, 700, 900, 1100, 1300$ K, the RDF changes correspond separately with the corresponding decrease in the number of crystallographic units from 12,514 atoms to 12,496, 12,462, 12,389, 12,306, 12,137 atoms (Table 1). Moreover, the size of the alloy has a constant value $r = 2.475$ Å, and the total energy of the system decrease from $E_{\text{tot}} = -58,263$ eV to $E_{\text{tot}} = -57,941, -57,610, -57,275, -56,938, -56,630$ eV (Table 1). The obtained results show that, when increased the temperature with $\text{Fe}_{63}\text{Ni}_{32}\text{Co}_5$ alloy of 13,500 atoms, the number of crystallographic units decreases, and Amor increases, indicating that $\text{Fe}_{63}\text{Ni}_{32}\text{Co}_5$ alloy of 13,500 atoms decreases, the crystallinity increase, and transfer gradually to the liquid state.

In addition, the relationship between temperature and total energy of the system has a close relationship with each other when increasing temperature leads to increased energy (according to Figure 4).

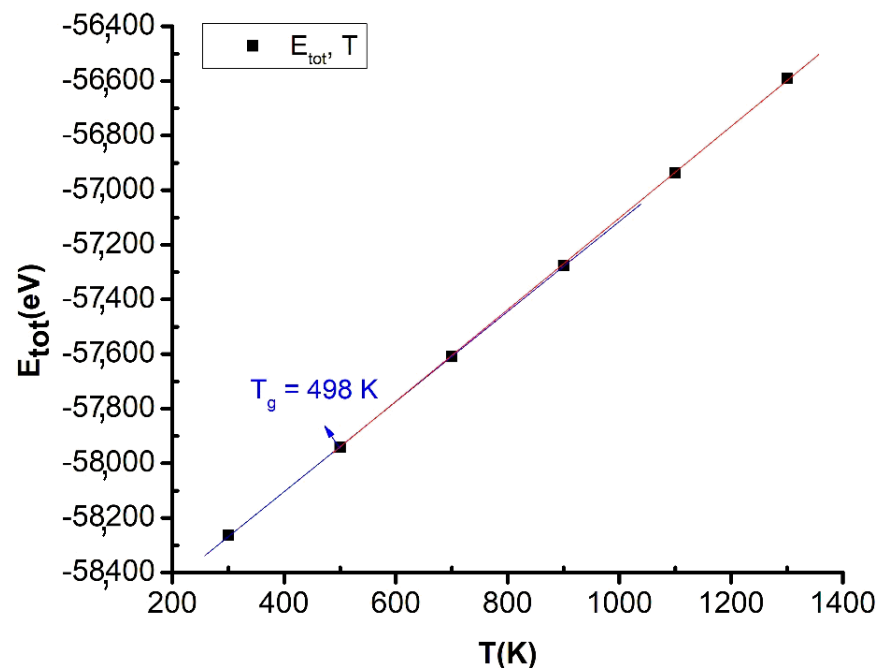


Figure 4. Phase transition of $\text{Fe}_{63}\text{Ni}_{32}\text{Co}_5$ alloy in the function of the temperature.

The results show that the relationship between T , E_{tot} has almost linear values and is interrupted at the point with the value $T = 498$ K. This point is called the glass point or glass temperature (T_g), $T = T_g = 498$ K. Moreover, some studies by the simulation study [22] confirmed that the cause of this phase transition is the size effect (surface effect). The obtained results are completely consistent with the experimental results with $T_g = 498$ K [77]. Based on these results, a major contribution to future experimental studies is determining the glass temperature of 3-component alloys (Figure 4).

In addition, our computational studies show that, when increasing the concentration of Fe and Co doping, the crystallization process increases, and when increasing Ni, the crystallization process decreases. Similarly, increasing the number of atoms leads to an increase in the crystallization process, and as the temperature increases, the crystallization process decreases. These results show that, with Fe, Ni, and Co 3-metal alloys, the bond lengths are constant, while the energy increases with increasing temperature, and decreases with increasing of the number of atoms. These results can be applied in the manufacturing of magnetic nano-alloy materials.

4. Conclusions

In this work, the structural characteristics, phase transition, and crystallization of $\text{Fe}_{1-x-y}\text{Ni}_x\text{Co}_y$ alloy under the influence of various factors (such as doping concentration, number of atoms, and temperature) were investigated. The obtained results show that in the $\text{Fe}_{1-x-y}\text{Ni}_x\text{Co}_y$ alloy always exist 03 metals Fe, Ni, and Cu (that are distributed quite evenly according to the ratio of tap phase concentration). In $\text{Fe}_{1-x-y}\text{Ni}_x\text{Co}_y$ alloy, there are always six types of links, Fe–Fe, Fe–Ni, Fe–Co, Ni–Ni, Ni–Co, and Co–Co. The structural features such as length (r), height of the radial distribution function $g(r)$ of links Fe–Fe, Fe–Ni, Ni–Co has a constant value such as $r = 2.475$ Å, and $g(r)$ changes (from $g(r)_{\text{Fe–Ni}} = 6.42$ to $g(r)_{\text{Fe–Ni}} = 7.32$, $g(r)_{\text{Fe–Co}} = 6.60$ to $g(r)_{\text{Fe–Co}} = 8.20$, $g(r)_{\text{Ni–Co}} = 6.97$ to $g(r)_{\text{Ni–Co}} = 7.35$) with a change of doping concentration Fe, Co. The result shows that when the increase of Fe and Co doping concentrations, the crystallization process increases corresponding with $\text{Fe}_5\text{Ni}_{32}\text{Co}_{63}$, and $\text{Fe}_{63}\text{Ni}_{32}\text{Co}_5$ alloy. Moreover, with the increase of Ni, the crystallization process decreases corresponding with $\text{Fe}_{33.4}\text{Ni}_{33.3}\text{Co}_{33.3}$ alloy. These results correspond with the number of structural units: FCC decreases and increases, HCP increases and decreases, BCC increases and decreases, Amor increases and decreases, and l decreases from $l = 5.34$ nm to $l = 5.33$ nm, E_{tot} increases from $E_{\text{tot}} = -58,189$ eV to $-57,932$ and $-58,263$ eV. In particular, $\text{Fe}_{63}\text{Ni}_{32}\text{Co}_5$ is the alloy with the highest crystallization caused by the interaction between electronic structures. Similarly, an increase in the number of atoms leads to an increase in crystallization, and an increase in temperature leads to a decrease in crystallization. Furthermore, computational results highlighted the glass temperature of $\text{Fe}_{63}\text{Ni}_{32}\text{Co}_5$ alloy has the value of $T_g = 498$ K, which is in accordance with experimental results. The obtained results serve as a basis for experimental studies in developing new magnetic materials in the future.

Author Contributions: D.N.T.: conceptualization, methodology, validation, investigation, writing, original draft, writing—review and editing, data curation, validation. V.C.L.: data curation, writing, and editing. Ş.T.: data curation, writing, review, editing, funding acquisition, project administration. All authors have read and agreed to the published version of the manuscript.

Funding: This research received no external funding.

Data Availability Statement: The data that supports the findings of this study are available from the corresponding author upon reasonable request.

Conflicts of Interest: The authors declare no conflict of interest.

References

1. Liu, W.H.; Wu, Y.; He, J.Y.; Nieh, T.G.; Lu, Z.P. Grain growth and the Hall–Petch relationship in a high-entropy FeCrNiCoMn alloy. *Scr. Mater.* **2013**, *68*, 526. [\[CrossRef\]](#)
2. Kozak, R.; Sologubenko, A.; Steurer, W. Single-phase high-entropy alloys—An overview. *Z. Für Krist. Cryst. Mater.* **2015**, *230*, 55–68. [\[CrossRef\]](#)
3. Li, Z.; Raabe, D. Strong, and Ductile Non-equiatom High-Entropy Alloys: Design, Processing, Microstructure, and Mechanical Properties. *JOM* **2017**, *69*, 2099–2106. [\[CrossRef\]](#) [\[PubMed\]](#)
4. Otto, F.; Yang, Y.; Bei, H.; George, E.P. Relative effects of enthalpy and entropy on the phase stability of equiatom high-entropy alloys. *Acta Mater.* **2013**, *61*, 2628–2638. [\[CrossRef\]](#)
5. Min, Z.; Jin-xiong, H.; Hui-jun, Y.; Ya-qin, T.; Xue-jiao, W.; Shi, X.-H.; Guo, R.-P.; Qiao, J.W. Tensile strength prediction of dual-phase Al_{0.6}CoCrFeNi high-entropy alloys. *Int. J. Miner. Metall. Mater.* **2020**, *27*, 1341–1346.
6. Yeh, J.W.; Chen, S.K.; Lin, S.J.; Gan, J.Y.; Chin, T.S.; Shun, T.T.; Tsau, C.H.; Chang, S.Y. Nanostructured high-entropy alloys with multiple principal elements: Novel alloy design concepts and outcomes. *Adv. Eng. Mater.* **2004**, *6*, 299–303. [\[CrossRef\]](#)
7. Cantor, B.; Chang, I.; Knight, P.; Vincent, A. Microstructural development in equiatom multicomponent alloys. *Mater. Sci. Eng.* **2004**, *375*, 213–218. [\[CrossRef\]](#)
8. Zhang, Y.; Zuo, T.T.; Tang, Z.; Gao, M.C.; Dahmen, K.A.; Liaw, P.K.; Lu, Z.P. Microstructures and properties of high-entropy alloys. *Prog. Mater. Sci.* **2014**, *61*, 1–93. [\[CrossRef\]](#)
9. Yuan, Y.; Wu, Y.; Tong, X.; Zhang, H.; Wang, H.; Liu, X.; Ma, L.; Suo, H.; Lu, Z. Rare-earth high-entropy alloys with giant magnetocaloric effect. *Acta Mater.* **2017**, *125*, 481–489. [\[CrossRef\]](#)
10. Gludovatz, B.; Hohenwarter, A.; Thurston, K.V.; Bei, H.; Wu, Z.; George, E.P.; Ritchie, R.O. Exceptional damage-tolerance of a medium-entropy alloy CrCoNi at cryogenic temperatures. *Nat. Commun.* **2016**, *7*, 10602. [\[CrossRef\]](#)
11. Li, Z.; Körmann, F.; Grabowski, B.; Neugebauer, J.; Raabe, D. Ab initio assisted design of quinary dual-phase high-entropy alloys with transformation-induced plasticity. *Acta Mater.* **2017**, *136*, 262–270. [\[CrossRef\]](#)
12. Laplanche, G.; Kostka, A.; Reinhart, C.; Hunfeld, J.; Eggeler, G.; George, E. Reasons for the superior mechanical properties of medium-entropy CrCoNi compared to high-entropy CrMnFeCoNi. *Acta Mater.* **2017**, *128*, 292–303. [\[CrossRef\]](#)
13. Miao, J.; Slone, C.; Smith, T.; Niu, C.; Bei, H.; Ghazisaeidi, M.; Pharr, G.; Mills, M.J. The evolution of the deformation substructure in a Ni-Co-Cr equiatom solid solution alloy. *Acta Mater.* **2017**, *132*, 35–48. [\[CrossRef\]](#)
14. Zhang, Z.; Sheng, H.; Wang, Z.; Gludovatz, B.; Zhang, Z.; George, E.P.; Yu, Q.; Mao, S.X.; Ritchie, R.O. Dislocation mechanisms and 3D twin architectures generate exceptional strength-ductility-toughness combination in CrCoNi medium-entropy alloy. *Nat. Commun.* **2017**, *8*, 14390. [\[CrossRef\]](#)
15. Zhao, Y.; Yang, T.; Tong, Y.; Wang, J.; Luan, J.; Jiao, Z.; Chen, D.; Yang, Y.; Hu, A.; Liu, C. Heterogeneous precipitation behavior and stacking-fault-mediated deformation in a CoCrNi-based medium-entropy alloy. *Acta Mater.* **2017**, *138*, 72–82. [\[CrossRef\]](#)
16. Zhang, Z.; Mao, M.; Wang, J.; Gludovatz, B.; Zhang, Z.; Mao, S.X.; George, E.P.; Yu, Q.; Ritchie, R.O. Nanoscale origins of the damage tolerance of the high-entropy alloy CrMnFeCoNi. *Nat. Commun.* **2015**, *6*, 10143. [\[CrossRef\]](#)
17. Dung, N.T.; Van, C.L. Effects of Number of Atoms, Shell Thickness, and Temperature on the Structure of Fe Nanoparticles Amorphous by Molecular Dynamics Method. *Adv. Civ. Eng.* **2021**, *2021*, 9976633.
18. Kien, P.H.; Lan, M.T.; Dung, N.T.; Hung, P.K. Annealing study of amorphous bulk and nanoparticle iron using molecular dynamics simulation. *Int. J. Mod. Phys. B* **2014**, *28*, 1450155. [\[CrossRef\]](#)
19. Dung, N.T.; Chinh, C.N.; Vinh, H.T. Molecular dynamics study of microscopic structures, phase transitions and dynamic crystallization in Ni nanoparticles. *RSC Adv.* **2017**, *7*, 25406–25413.
20. Hue, D.; Thi, M.; Gelu, C.; Hoc, N.Q.; Dung, N.T. Influence of heating rate, temperature, pressure on the structure, and phase transition of amorphous Ni material: A molecular dynamics study. *Heliyon* **2020**, *6*, e05548.
21. Tuan, T.Q.; Dung, N.T. Molecular dynamics factors affecting on the structure, phase transition of Al bulk. *Phys. B Condens. Matter* **2019**, *570*, 116–121.
22. Dung, N.T.; Van, C.L.; Țălu, Ș. Molecular dynamics simulation of bulk Cu material under various factors. *Appl. Sci.* **2022**, *12*, 4437.
23. Schneeweiss, O.; Friák, M.; Dudová, M.; Holec, D.; Šob, M.; Kriegner, D.; Holý, V.; Beran, P.; George, E.P.; Neugebauer, J. Magnetic properties of the CrMnFeCoNi highentropy alloy. *Phys. Rev. B* **2017**, *96*, 014437. [\[CrossRef\]](#)
24. Miracle, D.B.; Senkov, O.N. A critical review of high entropy alloys and related concepts. *Acta Mater.* **2017**, *122*, 448. [\[CrossRef\]](#)
25. Abdelhadi, N.; Rachid, T.; Noureddine, M. Design, and modeling of solenoid inductor integrated with FeNiCo in high frequency. *Telkommnika Telecommun. Comput. Electron. Control.* **2020**, *18*, 1746–1753.
26. Ding, Q.; Fu, X.; Chen, D.; Bei, H.; Gludovatz, B.; Li, J.; Zhang, Z.; George, E.P.; Yu, Q.; Zhu, T.; et al. Real-time nanoscale observation of deformation mechanisms in CrCoNi-based medium-to high-entropy alloys at cryogenic temperatures. *Mater. Today* **2019**, *25*, 21–27. [\[CrossRef\]](#)
27. Homnawang, N. Surface Micromachined Arch-Shape On-Chip 3-D Solenoid Inductors for High-frequency applications. *J. Micro Nanolithogr.* **2003**, *2*, 275–281.
28. Mostowski, J.; Trippenbach, M.; Van, C.L. Phase Space Approach to Two-electron Atom Ionisation. In Proceedings of the Fourth International Conference on Multiphoton Processes, Boulder, CO, USA, 13–17 July 1987.
29. Satoh, A. *Introduction to Practice of Molecular Simulation*; Elsevier Inc.: Amsterdam, The Netherlands, 2011.
30. Trippenbach, M.; Thesis, D. Center of Theoretical Physics. *Pol. Acad. Sci.* **1987**, *1*, 15–92.

31. Van, C.L.; Goldstein, P. *Concise Course in Nonlinear Partial Differential Equations*; Uniwersytetu Zielonogórskiego: Zielona Góra, Poland, 2008.
32. Dung, N.T. Influence of impurity concentration, atomic number, temperature and tempering time on microstructure and phase transformation of $\text{Ni}_{1-x}\text{Fe}_x$ ($x = 0.1, 0.3, 0.5$) nanoparticles. *Mod. Phys. Lett. B* **2018**, *32*, 1850204. [[CrossRef](#)]
33. Tuan, T.Q.; Dung, N.T. Effect of heating rate, impurity concentration of Cu, atomic number, temperatures, time annealing temperature on the structure, crystallization temperature, and crystallization process of $\text{Ni}_{1-x}\text{Cu}_x$ bulk; $x = 0.1, 0.3, 0.5, 0.7$. *Int. J. Mod. Phys. B* **2018**, *32*, 1830009. [[CrossRef](#)]
34. Dung, N.T.; Van, C.L. Factors affecting the depth of the Earth's surface on the heterogeneous dynamics of $\text{Cu}_{1-x}\text{Ni}_x$ alloy, $x = 0.1, 0.3, 0.5, 0.7, 0.9$ by Molecular Dynamics simulation method. *Mater. Today Commun.* **2021**, *29*, 102812.
35. Dung, N.T.; Phuong, N.T. Molecular dynamic study on factors influencing the structure, phase transition, and crystallization process of NiCu_{6912} nanoparticle. *Mater. Chem. Phys.* **2020**, *250*, 123075.
36. Dung, N.T.; Phuong, N.T. Factors affecting the structure, phase transition, and crystallization process of AlNi nanoparticles. *J. Alloy Compd.* **2020**, *812*, 152133.
37. Long, V.C.; Van, D.Q.; Dung, N.T. Ab Initio Calculations on the Structural and Electronic Properties of AgAu Alloys. *ACS Omega* **2020**, *5*, 31391–31397. [[CrossRef](#)]
38. Dung, N.T.; Cuong, N.C.; Van, D.Q. Study on the Effect of Doping on Lattice Constant and Electronic Structure of Bulk AuCu by the Density Functional Theory. *J. Multiscale Model.* **2020**, *11*, 2030001.
39. Tuan, T.Q.; Van, C.L.; Tãlu, Ş.; Dung, N.T. Molecular Dynamics Study on the Crystallization Process of Cubic Cu-Au Alloy. *Appl. Sci.* **2022**, *12*, 946.
40. Dung, N.T.; Van, C.L.; Tãlu, Ş. The Structure and Crystallizing Process of NiAu Alloy: A Molecular Dynamics Simulation Method. *J. Compos. Sci.* **2021**, *5*, 18.
41. Vu, Q.-T.; Tran, T.-T.-D.; Nguyen, T.-C.; Nguyen, T.V.; Nguyen, H.; Vinh, P.V.; Nguyen-Trong, D.; Dinh Duc, N.; Nguyen-Tri, P. DFT Prediction of Factors Affecting the Structural Characteristics, the Transition Temperature and the Electronic Density of Some New Conjugated Polymers. *Polymers* **2020**, *12*, 1207. [[CrossRef](#)]
42. Dung, N.T.; Van, C.L.; Phu, N.D.; Tãlu, Ş. A molecular dynamics study concerning the effect of high-temperature and high-pressure on the structure and phase transition of Fe_2O_3 material. *AIMS Mater. Sci.* **2022**, *9*, 406–429.
43. Dung, N.T.; Van, C.L.; Tãlu, Ş. The Study of the Influence of Matrix, Size, Rotation Angle, and Magnetic Field on the Isothermal Entropy, and the Né el Phase Transition Temperature of Fe_2O_3 Nanocomposite Thin Films by the Monte-Carlo Simulation Method. *Coatings* **2021**, *11*, 1209.
44. Leung, P.K.; Wright, J.G. Structural investigations of amorphous transition element films: II. chromium, iron, manganese and nickel. *Philos. Mag.* **1974**, *30*, 995–1008. [[CrossRef](#)]
45. Hoang, V.V.; Cuong, N.H. Local icosahedral order and thermodynamics of simulated amorphous Fe. *Phys. B Condens. Matter* **2009**, *404*, 340–346. [[CrossRef](#)]
46. Ma, P.W.; Dudarev, S.L.; Semenov, A.A.; Woo, C.H. Temperature for a dynamic spin ensemble. *Phys. Review. E Stat. Nonlinear Soft Matter Phys.* **2010**, *82*, 031111. [[CrossRef](#)] [[PubMed](#)]
47. Dung, N.T.; Kien, P.H.; Phuong, N.T. Simulation on the Factors Affecting the Crystallization Process of FeNi Alloy by Molecular Dynamics. *ACS Omega* **2019**, *4*, 14605–14612.
48. Gubin, S.P.; Koksharov, Y.A.; Khomutov, G.B.; Yurkov, G.Y. Magnetic nanoparticles: Preparation, structure and properties. *Russ. Chem. Rev.* **2005**, *74*, 489–520. [[CrossRef](#)]
49. Ichikawa, T. Electron diffraction study of the local atomic arrangement in amorphous iron and nickel films. *Phys. Status Solidi A* **1973**, *19*, 707–716. [[CrossRef](#)]
50. Lauriat, J.-P. Study by X-ray and neutron diffraction of the structure of Ex-carbonyl amorphous iron. *J. Non-Cryst. Solids* **1983**, *55*, 77–91. [[CrossRef](#)]
51. Zhao, W.; Gu, J.; Zhang, L.; Chen, H.; Shi, J. Fabrication of Uniform Magnetic Nanocomposite Spheres with a Magnetic Core/Mesoporous Silica Shell Structure. *J. Am. Chem. Soc.* **2005**, *127*, 8916–8917. [[CrossRef](#)]
52. Cao Long, V.; Saraç, U.; Baykul, M.C.; Trong, L.D.; Tãlu, Ş.; Nguyen Trong, D. Electrochemical Deposition of Fe-Co-Ni Samples with Different Co Contents and Characterization of Their Microstructural and Magnetic Properties. *Coatings* **2022**, *12*, 346. [[CrossRef](#)]
53. Spearot, D.E.; Tschopp, M.A.; Jacob, K.I.; McDowell, D.L. Tensile strength of $\langle 100 \rangle$ and $\langle 110 \rangle$ tilt bicrystal copper interfaces. *Acta Mater.* **2007**, *55*, 705–714. [[CrossRef](#)]
54. Tschopp, M.A.; Spearot, D.E.; McDowell, D.L. Atomistic simulations of homogeneous dislocation nucleation in single crystal copper. *Model. Simul. Mater. Sci. Eng.* **2007**, *15*, 693–709. [[CrossRef](#)]
55. Yanqiu, Z.; Shuyong, J. Atomistic mechanisms for temperature-induced crystallization of amorphous copper based on molecular dynamics simulation. *Comput. Mater. Sci.* **2018**, *151*, 25–33.
56. Foiles, S.M.; Baskes, M.I.; Daw, M.S. Embedded-atom-method functions for the FCC metals Cu, Ag, Au, Ni, Pd, Pt, and their alloys. *Phys. Rev. B.* **1986**, *33*, 7983. [[CrossRef](#)]
57. Mishin, Y.; Farkas, D.; Mehl, M.J. Papaconstantopoulos: Interatomic potentials for monoatomic metals from experimental data and ab initio calculations. *Phys. Rev. B* **1999**, *59*, 3393. [[CrossRef](#)]

58. Farkas, D.; Mutasa, B.; Vailhe, C.; Ternes, K. Interatomic potentials for B2 nial and martensitic phases. *Modell. Simul. Mater. Sci. Eng.* **1995**, *3*, 201. [[CrossRef](#)]
59. Farkas, D.; Jones, C. Interatomic potentials for ternary Nb–Ti–Al alloys. *Modell. Simul. Mater. Sci. Eng.* **1996**, *4*, 23. [[CrossRef](#)]
60. Farkas, D.; Roqueta, D.; Vilette, A.; Ternes, K. Atomistic simulations in ternary Ni-Ti-Al alloys. *Modell. Simul. Mater. Sci. Eng.* **1996**, *4*, 359. [[CrossRef](#)]
61. Farkas, D.; Schon, C.G.; De Lima, M.S.F.; Goldenstein, H. Embedded atom computer simulation of lattice distortion and dislocation core structure and mobility in Fe-Cr alloys. *Acta Mater.* **1996**, *44*, 409. [[CrossRef](#)]
62. Plimpton, S. Fast parallel algorithms for short-range molecular dynamics. *J. Comput. Phys.* **1995**, *117*, 1–19. [[CrossRef](#)]
63. Stukowski, A. Visualization, and analysis of atomistic simulation data with OVITO—the open visualization tool. *Modell. Simul. Mater. Sci. Eng.* **2010**, *18*, 015012. [[CrossRef](#)]
64. Farkas, D.; Caro, A. Model interatomic potentials and lattice strain in a high-entropy alloy. *J. Mater. Res.* **2018**, *1*, 1–8. [[CrossRef](#)]
65. Song, C.; Lin, T.; He, P.; Jiao, Z.; Tao, J.; Ji, Y. Molecular dynamics simulation of linear friction welding between dissimilar Ti-based alloys. *Comput. Mater. Sci.* **2014**, *83*, 35–38. [[CrossRef](#)]
66. Available online: https://en.wikipedia.org/wiki/Radial_distribution_function (accessed on 10 June 2022).
67. Lu, T.; Niu, G.J.; Xu, Y.; Wang, J.; An, Z.; Liu, H.; Zhou, H.; Ding, F.; Luo, G.N.; Li, X.C. Molecular dynamics study of the diffusion properties of H in Fe with point defects. *Fusion Eng. Des.* **2016**, *113*, 340–345. [[CrossRef](#)]
68. Stukowski, A.; Albe, K. Extracting dislocations and non-dislocation crystal defects from atomistic simulation data. *Model. Simul. Mater. Sci. Eng.* **2010**, *18*, 085001. [[CrossRef](#)]
69. Tsuzuki, H.; Branicio, P.S.; Rino, J.P. Structural characterization of deformed crystals by analysis of common atomic neighborhood. *Comput. Phys. Commun.* **2007**, *177*, 518–523. [[CrossRef](#)]
70. Stukowski, A. Structure identification methods for atomistic simulations of crystalline materials. *Modeling Simul. Mater. Sci. Eng.* **2012**, *20*, 045021. [[CrossRef](#)]
71. Sankaranarayanan, S.K.R.S.; Bhethanabotla, V.R.; Joseph, B. Molecular dynamics simulation study of the melting of Pd-Pt nanoclusters. *Phys. Rev. B* **2005**, *71*, 195415. [[CrossRef](#)]
72. Honeycutt, J.D.; Andersen, H.C. Molecular dynamics study of melting and freezing of small lennard-jones clusters. *J. Phys. Chem.* **1987**, *91*, 4950–4963. [[CrossRef](#)]
73. Ali, R.; Kamran, B. Identification of crystal structures in atomistic simulation by predominant common neighborhood analysis. *Comput. Mater. Sci.* **2017**, *126*, 182–190.
74. Xu, Y.H.; Wang, J.P. Direct Gas-phase synthesis of heterostructured nanoparticles through phase separation and surface segregation. *Adv. Mater.* **2008**, *20*, 994–999. [[CrossRef](#)]
75. Nosé, S. A unified formulation of the constant temperature molecular dynamics methods. *J. Chem. Phys.* **1984**, *81*, 511–519. [[CrossRef](#)]
76. Hoover, W.G. Canonical dynamics: Equilibrium phase-space distributions. *Phys. Rev. A* **1985**, *31*, 1695–1697. [[CrossRef](#)]
77. Nisheeth, K.P.; Vinod, K. Microstructure and magnetic properties of equiatomic FeNiCo alloy synthesized by mechanical alloying. *J. Mater Sci: Mater Electron.* **2015**, *26*, 10109–10118.